AGU PUBLICATIONS

Geophysical Research Letters

RESEARCH LETTER
10.1002/2016GL071964

Key Points:
- Remote triggering in geothermal fields is different from surrounding areas
- Geothermal production affects subsurface fracture network within geothermal fields
- Differential pore pressure primarily controls remote triggering in geothermal areas

Supporting Information:
- Supporting Information S1

Correspondence to:
Q. Zhang,
qizhang@caltech.edu

Citation:
Zhang, Q., G. Lin, Z. Zhan, X. Chen, Y. Qin, and S. Wdowinski (2017), Absence of remote earthquake triggering within the Coso and Salton Sea geothermal production fields, *Geophys. Res. Lett.*, *44*, 726–733, doi:10.1002/2016GL071964.

Received 15 NOV 2016
Accepted 4 JAN 2017
Accepted article online 7 JAN 2017
Published online 21 JAN 2017

Absence of remote earthquake triggering within the Coso and Salton Sea geothermal production fields

Qiong Zhang[1,2], Guoqing Lin[1], Zhongwen Zhan[2], Xiaowei Chen[3], Yan Qin[3], and Shimon Wdowinski[1,4]

[1]Department of Marine Geosciences, Rosenstiel School of Marine and Atmospheric Science, University of Miami, Miami, Florida, USA, [2]Seismological laboratory, California Institute of Technology, Pasadena, California, USA, [3]Geology and Geophysics, University of Oklahoma, Norman, Oklahoma, USA, [4]Department of Earth and Environment, Florida International University, Miami, Florida, USA

Abstract Geothermal areas are long recognized to be susceptible to remote earthquake triggering, probably due to the high seismicity rates and presence of geothermal fluids. However, anthropogenic injection and extraction activity may alter the stress state and fluid flow within the geothermal fields. Here we examine the remote triggering phenomena in the Coso geothermal field and its surrounding areas to assess possible anthropogenic effects. We find that triggered earthquakes are absent within the geothermal field but occur in the surrounding areas. Similar observation is also found in the Salton Sea geothermal field. We hypothesize that continuous geothermal operation has eliminated any significant differential pore pressure between fractures inside the geothermal field through flushing geothermal precipitations and sediments out of clogged fractures. To test this hypothesis, we analyze the pore-pressure-driven earthquake swarms, and they are found to occur outside or on the periphery of the geothermal production field. Therefore, our results suggest that the geothermal operation has changed the subsurface fracture network, and differential pore pressure is the primary controlling factor of remote triggering in geothermal fields.

1. Introduction

Earthquake remote triggering has been observed for decades, especially in geothermal and volcanic areas, such as Yellowstone [*Hill et al.*, 1993; *Husen et al.*, 2004], Long Valley [*Brodsky and Prejean*, 2005; *Aiken and Peng*, 2014], Geysers [*Hill et al.*, 1993; *Gomberg and Davis*, 1996; *Prejean et al.*, 2004], Salton Sea [*Gomberg et al.*, 2001; *Hough and Kanamori*, 2002], and Coso [*Hill et al.*, 1993; *Prejean et al.*, 2004; *Peng et al.*, 2010; *Aiken and Peng*, 2014]. These areas are susceptible to remote triggering, probably because they lie within tectonically active regions and active geothermal fluid or magma is present. In general, there are two kinds of physical models for explaining remote triggering: (1) preexisting faults that are critically loaded before the remote main shocks are brought to failure by dynamic stress [*Gomberg et al.*, 1997] and (2) interaction between active fluid and dynamic stress results in pore pressure change and fluid transport, which changes effective normal stress locally [*Hill et al.*, 1993; *Brodsky and Prejean*, 2005]. Between these two kinds of models, the first one has been regarded as the primary explanation, and the fluid-related triggering models are the secondary mechanisms. Thus, remote triggering has become a tool to diagnose whether the stress state in an area reaches the critical state [*van der Elst et al.*, 2013; *Taira et al.*, 2009].

In operational geothermal fields, anthropogenic activities of injecting and extracting fluid can perturb the stress state and affect the distribution of fluids within a porous medium, as shown by induced seismicity and rotation of stress orientations [*Martínez-Garzón et al.*, 2013]. Although the extent of these effects is still unknown, the in-situ conditions responding to remote earthquakes within the geothermal fields may be different from the surrounding areas without geothermal production. However, previous remote triggering studies in geothermal areas did not distinguish the actual operational geothermal fields from adjacent fault zones.

As one of the largest geothermal fields in the United States, the Coso geothermal field (CGF) has been in operation since 1987 with a net capacity of 270 MW [*Sass and Priest*, 2002]. It lies within the seismically active southern Walker Lane belt, which accommodates the relative motion between the Sierra Nevada block and the Basin and Range Province (Figure 1a). The Coso area sits under the transtensional stress regime with major strike-slip faults and small normal faults [*Reasenberg et al.*, 1980]. The Coso area has been reported to have

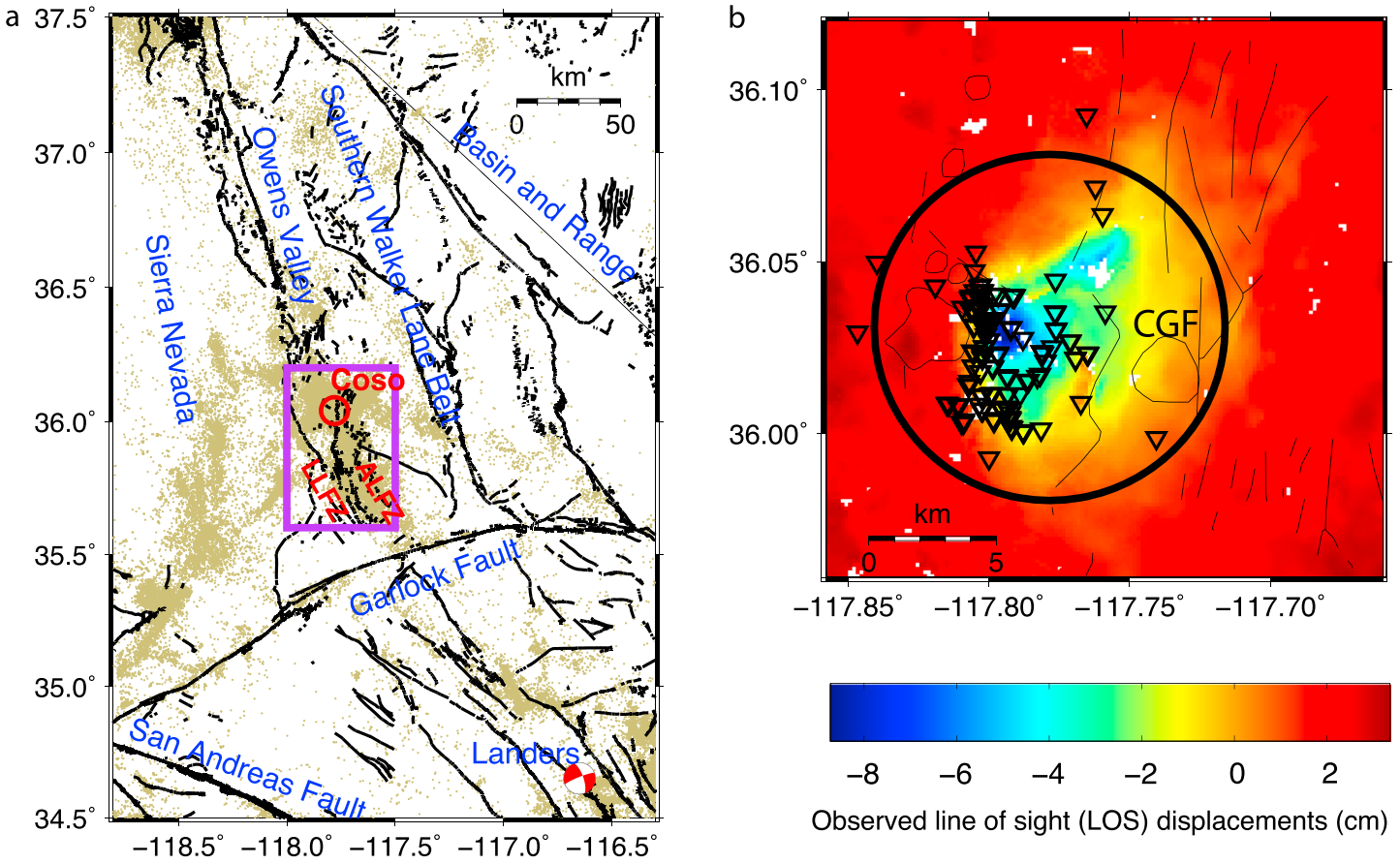

Figure 1. Tectonics and location of the Coso geothermal field (CGF). Circles in the two maps outline the location of the CGF. (a) Tectonic map showing the background seismicity (yellow dots) between 1981 and 2011 and the surface traces of the faults (black lines). Purple box encloses our entire study area, including the CGF and its vicinity. Most of the faults shown here are strike-slip, including the Little Lake Fault Zone (LLFZ) and the Airport Lake Fault Zone (ALFZ). The red beach ball represents the 1992 Landers earthquake. (b) Lateral extent of the CGF (black circle), as defined by the locations of the active injection and extraction wells (black triangles) for the geothermal operation and the observed land subsidence. Locations of the wells are obtained from the California Oil, Gas, and Geothermal Resources (DOGGR). Background is the subsidence between September 1993 and May 1996 from InSAR data, modified from Plate 1(c) in *Fialko and Simons* [2000].

triggering response following M > 7.0 earthquakes including the 1992 Landers earthquake [*Hill et al.*, 1993], the 2002 Denali earthquake [*Prejean et al.*, 2004], the 2005 Mendocino earthquake [*Aiken and Peng*, 2014], the 2010 Baja California earthquake [*Aiken and Peng*, 2014], and the 2010 Chile earthquake [*Peng et al.*, 2010]. In particular, the 1992 Landers earthquake triggered the most wide-spreading seismicity in Coso, at a spatial scale of hundreds of kilometers. To investigate the effects on stress state and subsurface fluid distribution within the geothermal reservoir, we revisit the triggering response in the Coso area (56×67 km^2, box in Figure 1a) following the Landers earthquake and conduct a fine-scale study of remote trigging to compare the triggering response within the Coso geothermal field (Figure 1) to that in its surrounding areas.

2. Methods

We use a relocation catalog for events between 1981 and 2011 in the Coso area [*Zhang and Lin*, 2014], which was obtained by using a new regional three-dimensional velocity model and differential travel times from waveform cross-correlation. The new absolute location uncertainties are 120 m in horizontal and 300 m in depth, while the relative location errors are smaller with 11 m in horizontal and 22 m in depth. In our study area, a total of 19 stations were operating between 1981 and 2011. In 1992, when the Landers earthquake occurred, 11 stations were available in our study area, and three of them were located within 15 km of the geothermal field. Over 94% of the relocated events were recorded by eight or more stations. We then calculate the magnitude of completeness Mc for the entire study area and the geothermal field. Following the method of the maximum curvature [*Wiemer and Wyss*, 2000], we compute Mc as the magnitude with the maximum

derivative of the Gutenberg-Richter frequency-magnitude curve without adding other smoothing parameters. We estimate the completeness magnitude Mc of this catalog to be 1.3 for the entire study area and 1.0 for the CGF (Figure S1 in the supporting information). Therefore, we use $M = 1.3$ as the threshold magnitude for the following analyses to ensure completeness within the entire study area.

Before analyzing the spatiotemporal distribution of the seismicity remotely triggered by the Landers earthquake, we decluster the full catalog to remove local aftershock sequences following the Reasenberg method [*Reasenberg*, 1985]. For each earthquake, the method first models its spatial and temporal extent based on the source dimension of the main shock and the Omori's law. Each event is then cross-correlated with other events to form clusters when they are proximate to each other in location and time. The cluster grows with more cross-correlated events. Events within a single cluster are dependent on each other and thus are regarded as an aftershock-related sequence. The largest event in each cluster is considered as the main shock and kept in the final declustered catalog. An example of declustering in Rose Valley (subarea 3) shows that the aftershock sequence of an Mw 4.1 main shock in February 1992 is removed, whereas the increased seismicity after the Landers earthquake is much less affected, suggesting that the increase is not a coincident aftershock sequence after some local earthquakes (Figure S2 in the supporting information).

We calculate the seismicity rate change for 30 days after the Landers earthquake relative to the background seismicity from 1987 to 1993 using the β-statistic [*Matthews and Reasenberg*, 1988; *Reasenberg and Simpson*, 1992; *Kilb et al.*, 2000; *Hill and Prejean*, 2007], which compares the difference between the observed and expected seismicity in 30 days, normalized by standard deviation of the expected seismicity. It can be expressed as [*Matthews and Reasenberg*, 1988; *Hill and Prejean*, 2007]

$$\beta(n_a, n_b, t_a, t_b) = \frac{n_a - E(n_a, n_b)}{\sqrt{\mathrm{var}(n_a, n_b)}} \tag{1}$$

where n_a and n_b are the numbers of earthquakes in the time period of t_a and t_b, respectively. $E(n_a, n_b)$ is the expected number of earthquakes in t_a based on the sample of background seismicity rate in t_b. $\mathrm{var}(n_a, n_b)$ denotes the variance of the number of earthquakes in t_a based on the sample of the background seismicity rate in t_b. The study area is gridded with blocks of 5×6 km^2, which are chosen to ensure relatively uniform seismicity in different blocks. Figure 2a shows the seismicity rate change for a 30 day time window. (The rate changes for 10 and 100 day windows are shown in Figure S3 in the supporting information.)

We also search for earthquake swarms and analyze their temporal migration for evidence of fluid-related pore-pressure propagation. We define swarms as sequences clustering in space and time but without clear main shocks. We search for swarms in our study area from the 1981-2011 relocated catalog [*Zhang and Lin*, 2014] following the method of *Zhang and Shearer* [2016]. The method first searches for the closest neighboring earthquakes in space and time for each earthquake, and clusters are identified when the number of closest neighbors is significantly more than the number of background events in larger space and time windows. A total of 156 clusters including 6415 events are identified in the Coso area. These clusters are then divided into swarm-like sequences and main shock-aftershock sequences by two measures: the timing of the largest event t_m normalized by the mean value of the occurrence time and the skewness of the moment release with time μ. The skewness value is defined as [*Roland and McGuire*, 2009; *Chen and Shearer*, 2011; *Zhang and Shearer*, 2016]

$$\mu = \frac{\sum_{i=1}^{N} \left(t_i - t^*\right)^3 M_i}{\sigma^3} \tag{2}$$

where t^* is the centroid occurrence time, M_i is the moment release, and σ is the standard deviation of central moment. A set of experimental cutoff values is applied to categorize clusters. Clusters with $t_m \geq 0.5$ and $\mu \leq 6$ are classified as swarm-like sequences, and clusters with $t_m < 0.5$ and $\mu > 6$ are classified as main shock-aftershock sequences.

We then analyze the space-time behavior of swarm sequences by fitting with two types of migration models, linear and diffusion migration. A linear migration, in which migrating distance, r, is linearly proportional to time t, often suggests a driving mechanism of aseismic slip [*Chen and Shearer*, 2011], whereas the migration front in the diffusion model follows $r = \sqrt{4\pi D t}$, where D is the hydraulic diffusivity [*Shapiro et al.*, 1997]. We determine which model is more favorable for each swarm sequence by comparing the residuals. Because these two models fit the migration front, the furthest migrating distance at each discretized time, it is possible

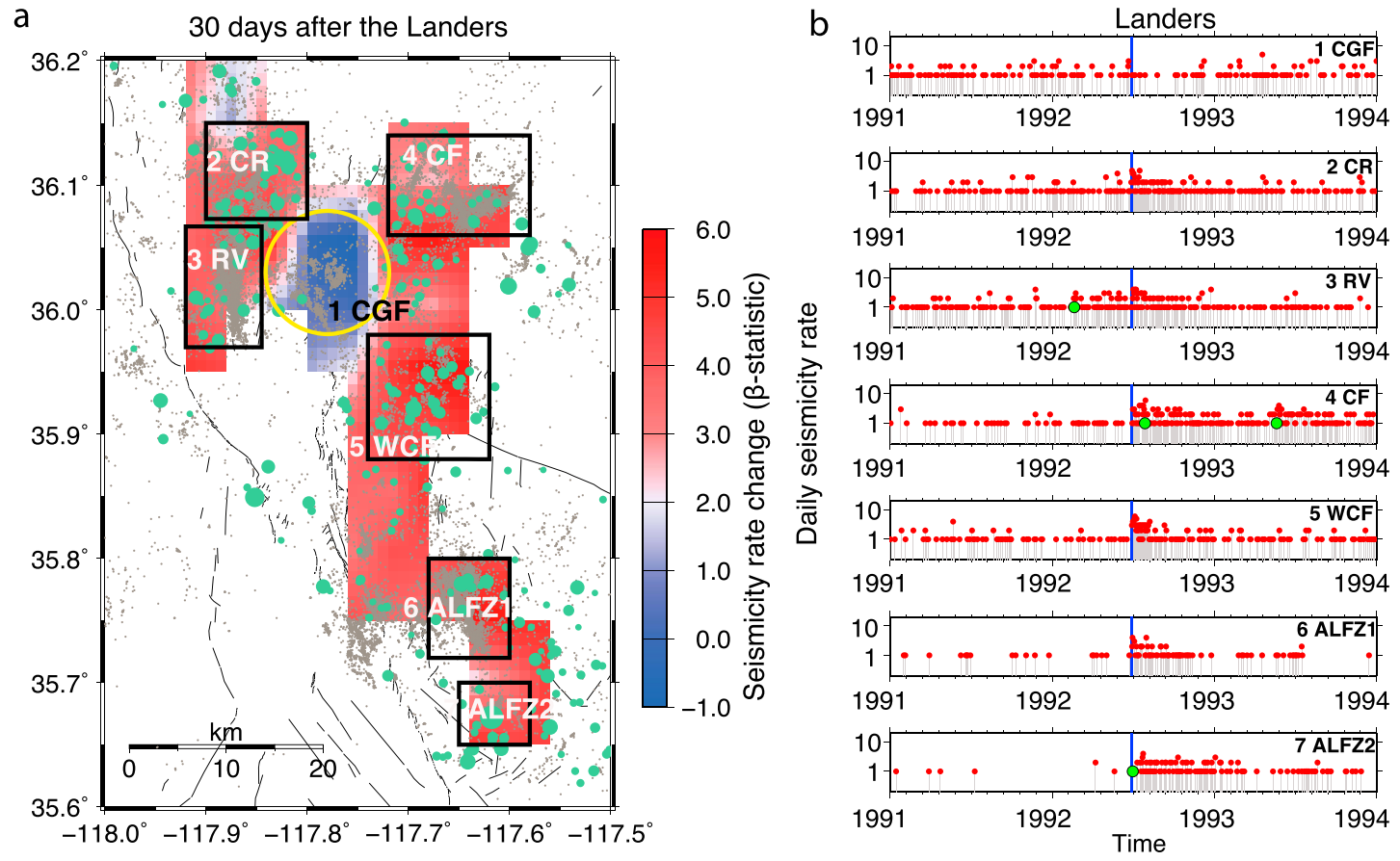

Figure 2. (a) Spatial distribution of the declustered seismicity (green circles) within 30 days following the Landers earthquake and the β-statistic of the seismicity rate change (colored grids), calculated relative to the background period 1987–1993. Based on the distribution of the background seismicity between 1981 and 2011 (grey dots), we assigned the Coso geothermal field (CGF) as subarea 1 and divided the adjacent area into six subareas, including the Coso Range (CR), Rose Valley (RV), Centennial Flat (CF), Wilson Canyon Fault (WCF), and Airport Lake Fault Zone (ALFZ). We masked out those grid blocks with too sparse background seismicity between 1987 and 1993. (b) Number of events per day in the seven subareas between 1991 and 1993. The 3 year time window was chosen to keep the detection criteria identical before and after the Landers earthquake. Red dots represent microearthquakes with $1.3 \leq Mw < 4.0$ in the declustered catalog and green dots for $Mw \geq 4.0$. Blue vertical lines mark the onset of the 1992 Landers earthquake.

that residuals in both models are large due to scattered data, in which cases we make the time-distance plot and visually check if any model is applicable. If neither model can explain the time-distance relationship, we regard the sequence without clear migration.

3. Results

3.1. Statistical Analysis of Seismicity Rate Change

The β values larger than 2 or smaller than −2 indicate significantly higher or lower seismicity rates than the background [*Reasenberg and Simpson*, 1992; *Hill and Prejean*, 2007]. The areas outside the geothermal field show high β values (up to 6), indicating wide-spreading triggering within 30 days (Figure 2a), consistent with the previous study [*Hill et al.*, 1993]. This increase can also be observed in other time windows (e.g., 10 days, Figure S3 in the supporting information) and becomes less significant after 100 days following the Landers earthquake (Figure S3 in the supporting information). However, we also observe an absence of seismicity rate change inside the geothermal field. During the time windows from 10 to 100 days after the Landers earthquake, the maximum and minimum β values in the CGF are 1.81 and −1, respectively, which fall in the typical statistical range of background seismicity and means that there is no significant increase or decrease of seismicity rate inside the geothermal field. The different β values within and outside the CGF suggest that the active geothermal field and its surrounding areas respond differently to seismic waves from the distant Landers earthquake.

In order to compare the spatiotemporal variation of the seismicity at consistent spatial scales, we assign the geothermal field as subarea 1 and divide the adjacent area into six subareas of similar sizes (black boxes in Figure 2a) based on the distribution of the background seismicity from 1981 to 2011. Figure 2b shows the time series for all the seven subareas between 1991 and 1993. We observe an abrupt increase in the seismicity rates after the Landers earthquake for all the six subareas outside the CGF. In contrast, the geothermal field itself appears unaffected by the Landers earthquake, which is consistent with our β statistic analysis above. We also calculate the Poissonian probability that the observed seismicity in the 30-day window following the Landers earthquake is indeed a dynamically triggered response. When the probability is less than 0.05, we reject the null hypothesis that the increased seismicity is a random occurrence. With 95% of confidence, our results indicate that the increased seismicity outside the geothermal field cannot be random occurrences (Table S1 in the supporting information). Although some smaller events may be missing from the regional catalog, they would not change the observation that inside and outside the geothermal field seismicity responded to the large remote earthquake differently based on the same detection criteria. In addition, the different triggering responses inside and outside the geothermal field are not artifact of the declustering process because the difference can also be observed from the raw catalog (Figure S4 in the supporting information).

3.2. Study of Pore-Pressure-Driven Swarms

Our results confirm that areas in the vicinity of but outside the producing geothermal field are susceptible to remote triggering. Here, however, we have clearly established the absence of remote triggering inside the CGF production area. Before we attempt to estimate the stress state, we first test the second kind of remote triggering model. Among the numerous fluid-related triggering models, the fracture unclogging model can be uniquely applied to geothermal fields in that the geothermal mineral precipitation and sediments lead to clogged fractures, which results in differential pore pressure within fracture network [*Brodsky et al.*, 2003; *Brodsky and Prejean*, 2005]. This fracture unclogging model has also been used as one of the explanations to the absence of remote triggering in Japan [*Harrington and Brodsky*, 2006]. We hypothesize that the continuous injection and extraction of geothermal fluid within the reservoir can disturb the clogged fracture and flush the blockages from fractures, which prevents the formation of differential pore pressure, while the fractures in natural settings remain clogged.

Since pore-pressure-driven migrating swarms suggest the presence of pore pressure gradient within subsurface fractures, the analysis of swarms can help test our hypothesis. A total of 71 swarms including 28 swarms with at least 20 events are found in our study area (Figure 3a). Swarms driven by pore pressure diffusion are only observed within tens of kilometers away from the CGF, but not inside the CGF (Figure 3a). These pore-pressure-driven swarms show a median hydraulic diffusivity of 0.5 m^2/s (Figure 3b), which falls in the range of typical hydraulic diffusivity values, $10^{-10} - 10^4$ m^2/s [*Manga and Wang*, 2007]. Four swarms are found at the edge of the CGF but without a clear migration pattern. The result is consistent with our hypothesis that pore pressure gradient exists within the clogged fractures outside the CGF. Hence, the correlation of remote triggering and pore-pressure-driven swarms suggests that differential fluid pore pressure could play an active role in controlling remote triggering in geothermal areas. Note that the absence of remote triggering might be also explained by the stress state model if the dynamic stress associated with the geothermal production is known. Our results also suggest that the geothermal operation has altered the subsurface fracture network within the CGF.

3.3. Background Seismicity Rate Analysis

Since areas of elevated background seismicity are commonly assumed to be close to critical stress state [*Hill and Prejean*, 2015], we further study the background seismicity rate inside and outside the CGF. We divide the background seismicity into a shallow layer (<3 km) that is associated with the geothermal operation process and a deeper layer confined between 3 and 15 km depth. Within the CGF, the seismicity rate in the deeper layer decreases following the onset of the geothermal operation in 1987 and remains low afterward (Figure 4). In contrast, the seismicity rate in the shallow layer keeps growing with the geothermal production and can be considered as induced seismicity, which has been proposed to result from reservoir contraction, thermoelastic and poroelastic effects [*Segall and Fitzgerald*, 1998]. While we observe that the CGF seismicity rates in the shallow and deeper layers diverge after the onset of the production, the stacked seismicity rate outside the CGF shows similar oscillation patterns for the shallow and deeper layers within the 30 year window. Without direct anthropogenic disturbance, the absence of remote triggering and the decreased background seismicity rate in the deeper layer within the CGF may indicate that the stress state is away from failure, probably due to reservoir unloading, reduced pore pressure, and/or increased precipitation, which may have implications for

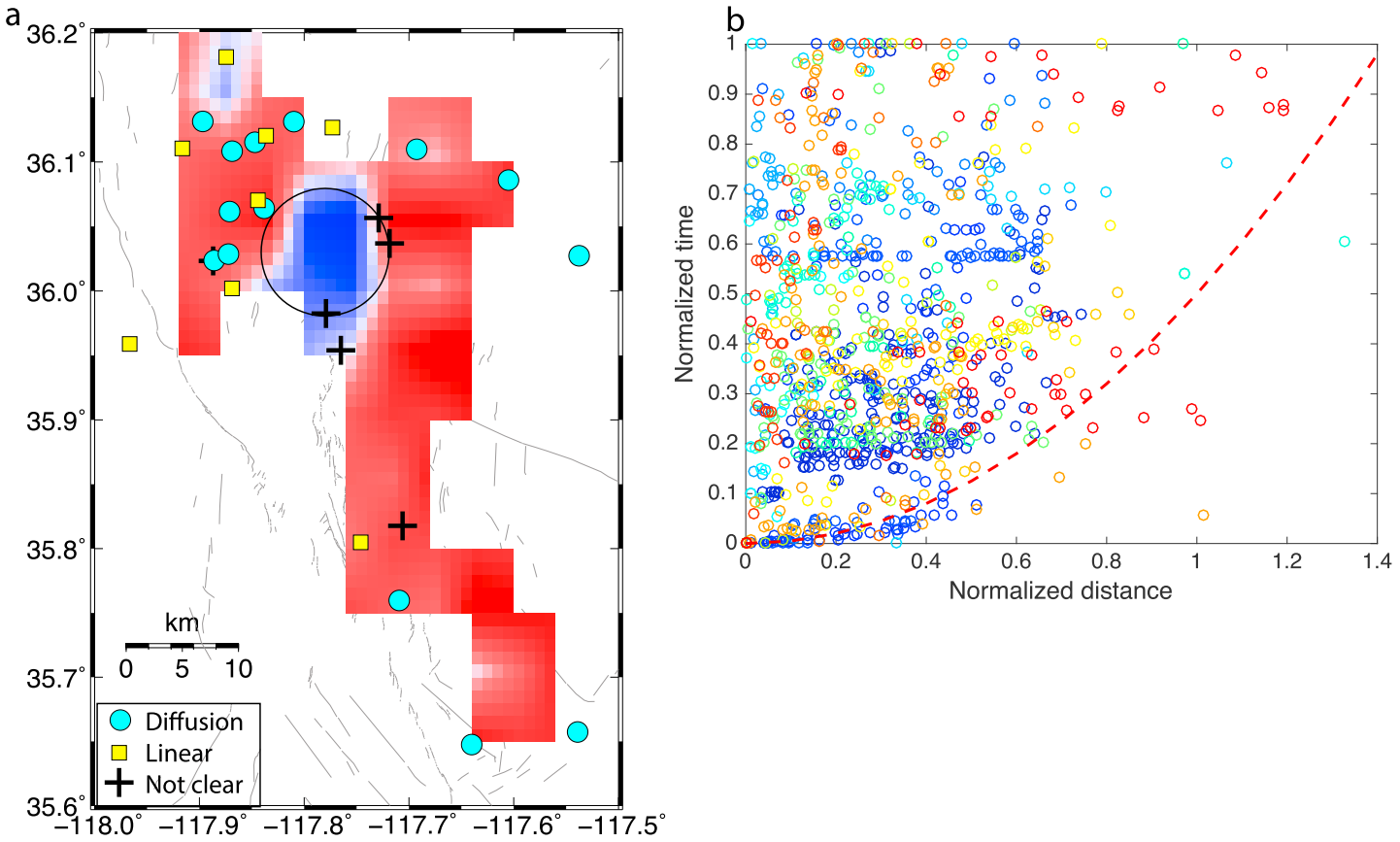

Figure 3. Spatial distribution and migration patterns of swarms. (a) Map of three types of earthquake swarms analyzed from the 1981–2011 relocation catalog. Each swarm contains more than 20 events. The swarms showing migration with hydraulic diffusion are denoted by blue circles. Squares and crosses denote swarms with linear migration and no obvious migration, respectively. The red and blue background colors are the same as in Figure 2. (b) Stacked time-distance plot of 14 swarms fitting to diffusion migration (blue circles in Figure 3a). The events in one swarm are denoted by the same color. The time is normalized by t_i, the maximum time for each swarm. The distance is normalized by $\sqrt{4\pi D_i}$ (D_i is the hydraulic diffusivity for each swarm) and then normalized by $\sqrt{t_i}$. The dashed line shows the migration front with the median diffusivity of 0.5 m^2/s.

induced seismic hazard because large earthquakes are more prone to occur in the crystalline basement than the sedimentary layer [*Walsh and Zoback*, 2015; *Zhang et al.*, 2013]. Note that we observe both an absence of remote triggering and an increase of background seismicity within the shallow producing layer. We cannot, however, infer the average stress state in this layer without some knowledge of the dynamic stress associated with geothermal production that results in the elevated induced seismicity rates.

3.4. Case Studies of More Main Shocks and the Salton Sea Geothermal Field

In order to check if the Landers earthquake is a special case for the remote triggering in the Coso area, we study the triggering responses to other remote large earthquakes. We search 22 main shocks from 1981 to 2011 with $M_s \geq 7.0$ and epicentral distance ≥100 km in the International Seismological Centre (ISC) catalog. Also, their expected Peak Ground Velocity (PGV) values are required to exceed 0.05 cm/s, which are calculated from PGV $= 2\pi/T \times 10^{M_s - 1.66\log_{10}A - 2}$, where T is the surface wave period, M_s is the surface wave magnitude, and A is the distance from the main shock to our study area [*Lay and Wallace*, 1995] (Figure S5a in the supporting information). We estimate the declustered seismicity rate change in the 30 days before and after each main shock using the β statistic. Among the 22 main shocks, the Landers earthquake shows the most significantly wide-spreading remote triggering in the Coso area (Figure S5b in the supporting information), probably because the Landers earthquake ruptured in a northern direction toward the Coso area. The stacked β value map of the other 21 main shocks suggests that there is no statistically significant seismicity rate change inside the CGF, while the observed seismicity rate increase occurs outside the CGF (Figure S5c in the supporting information).

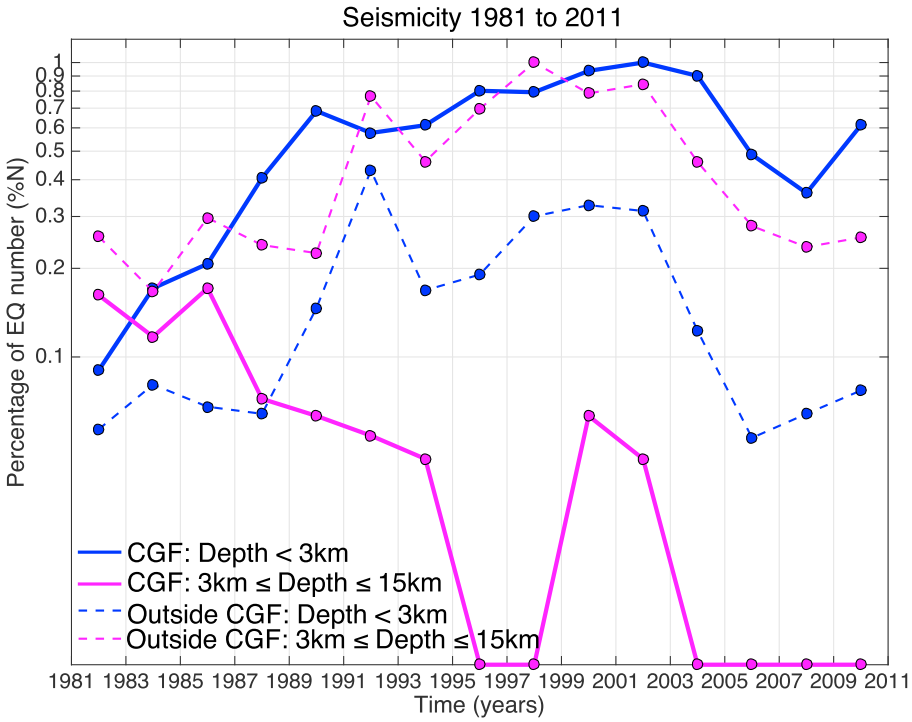

Figure 4. Background seismicity distribution within and outside the geothermal field. Solid lines denote seismicity rate within the geothermal field and dashed lines denote stacked rate of six subareas outside the geothermal field. Percentage of earthquake number (%N) is the number of earthquakes every 2 years for the time period of 1981 to 2011 normalized by the maximum seismicity rate, which are 111 and 546 for the CGF and six subareas outside the geothermal field, respectively. The reduction in the number of deeper earthquakes occurred in 1987 when the production operation began.

Similar to the CGF, the Salton Sea Geothermal Field (SSGF) located on the southeast shore of the Salton Sea in California is also characterized by transtensional tectonic regime with highly active seismicity, strong subsidence, and long-term geothermal fluid loss (Figure S6 in the supporting information) [*Brothers et al.*, 2009; *Brodsky and Lajoie*, 2013]. Here we use a relocated earthquake catalog [*Lin*, 2013] to examine the remote triggering in the Salton Sea area, which has been shown to respond to the 1999 Mw 7.1 Hector Mine earthquake [*Hough and Kanamori*, 2002; *Gomberg et al.*, 2001]. We conduct similar analyses of seismicity rate change as for the Coso area and show the β statistic and 1 year time series in Figure S7 in the supporting information. We observe increased seismicity within 5 km north and south of the SSGF, indicated by large β values (~6) within 4 days after the Hector Mine earthquake. However, the seismicity inside the SSGF did not show an abrupt increase. The remotely triggered earthquake sequence identified by a previous study [*Hough and Kanamori*, 2002] also falls outside the geothermal field. Therefore, the observed absence of remote triggering within CGF does not appear to be a special case.

4. Conclusions

In summary, we have studied the fine-scale remote triggering in two geothermal fields, the Coso Geothermal Field and the Salton Sea Geothermal Field, and their vicinities to assess the anthropogenic effect on the stress state and subsurface fracture network. We find that the geothermal production areas are less susceptible to remote triggering than the surrounding areas, which can be explained by reduced differential pore pressure resulting from fracture unclogging/flushing by geothermal operations (fluid extraction and injection). While the fault strength in the crystalline basement beneath the geothermal reservoir is increased, we cannot evaluate the stress state of the geothermal reservoir solely from remote triggering considering the effect of fracture unclogging. The effects of anthropogenic activities on fracture network and pore fluid pressure should be evaluated when diagnosing the stress state through remote triggering in anthropogenic settings. Although our observations show less susceptibility to remote triggering within the two geothermal fields,

tectonic stress will continue to accumulate to balance the decreased pore pressure. In addition, changes in injection volume or hydrological system may also alter the fracture network.

Acknowledgments
Geothermal injection and production data are obtained from the DOGGR (accessible from http://www.conservation.ca.gov/dog/geothermal). Catalog data for distant earthquakes are available from the ISC website (http://www.isc.ac.uk/iscbulletin/search/catalogue/). We thank the SCEDC for providing the local earthquake data. We thank the editor, Andrew Newman and two reviewers David P. Hill and Chastity Aiken for constructive comments that helped improve the manuscript. This paper benefited from discussion with Hiroo Kanamori and Michael Manga. We thank Heresh Fattahi for providing the InSAR results. This research work was supported by the National Science Foundation grant EAR-1447105 and partially supported by the SCEC grant 16071.

References

Aiken, C., and Z. Peng (2014), Dynamic triggering of microearthquakes in three geothermal/volcanic regions of California, *J. Geophys. Res. Solid Earth*, *119*, 6992–7009, doi:10.1002/2014JB011218.

Brodsky, E. E., and L. J. Lajoie (2013), Anthropogenic seismicity rates and operational parameters at the Salton Sea Geothermal field, *Science*, *341*(6145), 543–546.

Brodsky, E. E., and S. G. Prejean (2005), New constraints on mechanisms of remotely triggered seismicity at Long Valley Caldera, *J. Geophys. Res.*, *110*, B04302, doi:10.1029/2004JB003211.

Brodsky, E. E., E. Roeloffs, D. Woodcock, I. Gall, and M. Manga (2003), A mechanism for sustained groundwater pressure changes induced by distant earthquakes, *J. Geophys. Res.*, *108*(B8), 2390, doi:10.1029/2002JB002321.

Brothers, D., N. Driscoll, G. Kent, A. Harding, J. Babcock, and R. Baskin (2009), Tectonic evolution of the Salton Sea inferred from seismic reflection data, *Nat. Geosci.*, *2*(8), 581–584.

Chen, X., and P. Shearer (2011), Comprehensive analysis of earthquake source spectra and swarms in the Salton Trough, California, *J. Geophys. Res.*, *116*, B09309, doi:10.1029/2011JB008263.

Fialko, Y., and M. Simons (2000), Deformation and seismicity in the Coso geothermal area, Inyo County, California: Observations and modeling using satellite radar interferometry, *J. Geophys. Res.*, *105*(B9), 21,781–21,794.

Gomberg, J., and S. Davis (1996), Stress/strain changes and triggered seismicity at the Geysers, California, *J. Geophys. Res.*, *101*(B1), 733–749.

Gomberg, J., M. L. Blanpied, and N. Beeler (1997), Transient triggering of near and distant earthquakes, *Bull. Seismol. Soc. Am.*, *87*(2), 294–309.

Gomberg, J., P. Reasenberg, P. Bodin, and R. Harris (2001), Earthquake triggering by seismic waves following the Landers and Hector Mine earthquakes, *Nature*, *411*(6836), 462–466.

Harrington, R. M., and E. E. Brodsky (2006), The absence of remotely triggered seismicity in Japan, *Bull. Seismol. Soc. Am.*, *96*(3), 871–878.

Hill, D., and S. Prejean (2007), Dynamic triggering, in *Earthquake Seismology Treatise on Geophysics*, vol. 4, edited by H. Kanamori, pp. 257–291, Elsevier, Amsterdam.

Hill, D., and S. Prejean (2015), Dynamic triggering, in *Treatise on Geophysics*, 2nd ed., vol. 4, edited by G. Schubert, pp. 273–304, Elsevier, Amsterdam.

Hill, D., et al. (1993), Seismicity remotely triggered by the magnitude 7.3 Landers, California, earthquake, *Science*, *260*(5114), 1617–1623.

Hough, S. E., and H. Kanamori (2002), Source properties of earthquakes near the Salton Sea triggered by the 16 October 1999 m 7.1 Hector Mine, California, earthquake, *Bull. Seismol. Soc. Am.*, *92*(4), 1281–1289.

Husen, S., S. Wiemer, and R. B. Smith (2004), Remotely triggered seismicity in the Yellowstone National Park region by the 2002 Mw 7.9 Denali Fault earthquake, Alaska, *Bull. Seismol. Soc. Am.*, *94*(6B), S317–S331.

Kilb, D., J. Gomberg, and P. Bodin (2000), Triggering of earthquake aftershocks by dynamic stresses, *Nature*, *408*(6812), 570–574.

Lay, T., and T. C. Wallace (1995), *Modern Global Seismology*, vol. 58, Academic Press, San Diego, Calif.

Lin, G. (2013), Three-dimensional seismic velocity structure and precise earthquake relocations in the Salton Trough, southern California, *Bull. Seismol. Soc. Am.*, *103*(5), 2694–2708.

Manga, M., and C. Wang (2007), Earthquake hydrology, *Treatise Geophys.*, *4*(10), 293–320.

Martínez-Garzón, P., M. Bohnhoff, G. Kwiatek, and G. Dresen (2013), Stress tensor changes related to fluid injection at the Geysers geothermal field, California, *Geophys. Res. Lett.*, *40*, 2596–2601, doi:10.1002/grl.50438.

Matthews, M. V., and P. A. Reasenberg (1988), Statistical methods for investigating quiescence and other temporal seismicity patterns, *Pure Appl. Geophys.*, *126*(2–4), 357–372.

Peng, Z., D. P. Hill, D. R. Shelly, and C. Aiken (2010), Remotely triggered microearthquakes and tremor in central California following the 2010 Mw 8.8 Chile earthquake, *Geophys. Res. Lett.*, *37*, L24312, doi:10.1029/2010GL045462.

Prejean, S., D. Hill, E. Brodsky, S. Hough, M. Johnston, S. Malone, D. Oppenheimer, A. Pitt, and K. Richards-Dinger (2004), Remotely triggered seismicity on the United States West Coast following the Mw 7.9 Denali fault earthquake, *Bull. Seismol. Soc. Am.*, *94*(6B), S348–S359.

Reasenberg, P. (1985), Second-order moment of central California seismicity, 1969–1982, *J. Geophys. Res.*, *90*(B7), 5479–5495.

Reasenberg, P., W. Ellsworth, and A. Walter (1980), Teleseismic evidence for a low-velocity body under the Coso Geothermal Area, *J. Geophys. Res.*, *85*(B5), 2471–2483.

Reasenberg, P. A., and R. W. Simpson (1992), Response of regional seismicity to the static stress change produced by the Loma Prieta earthquake, *Science*, *255*(5052), 1687–1690.

Roland, E., and J. J. McGuire (2009), Earthquake swarms on transform faults, *Geophys. J. Int.*, *178*(3), 1677–1690.

Sass, J., and S. Priest (2002), Geothermal California: California claims the world's highest geothermal power output with potential for even more production with advanced techniques, *GRC Bull.*, *31*, 183–187.

Segall, P., and S. D. Fitzgerald (1998), A note on induced stress changes in hydrocarbon and geothermal reservoirs, *Tectonophysics*, *289*(1), 117–128.

Shapiro, S. A., E. Huenges, and G. Borm (1997), Estimating the crust permeability from fluid-injection-induced seismic emission at the KTB site, *Geophys. J. Int.*, *131*(2), F15–F18.

Taira, T., P. Silver, F. Niu, and R. Nadeau (2009), *Remote Triggering of Fault-Strength Changes on the San Andreas fault at Parkfield*, 636–639, vol. 461.

van der Elst, N. J., H. M. Savage, K. M. Keranen, and G. A. Abers (2013), Enhanced remote earthquake triggering at fluid-injection sites in the midwestern United States, *Science*, *341*(6142), 164–167.

Walsh, F. R., and M. D. Zoback (2015), Oklahoma's recent earthquakes and saltwater disposal, *Sci. Adv.*, *1*(5), e1500195.

Wiemer, S., and M. Wyss (2000), Minimum magnitude of completeness in earthquake catalogs: Examples from Alaska, the western United States, and Japan, *Bull. Seismol. Soc. Am.*, *90*(4), 859–869.

Zhang, Q., and G. Lin (2014), Three-dimensional Vp and Vp/Vs models in the Coso geothermal area, California: Seismic characterization of the magmatic system, *J. Geophys. Res. Solid Earth*, *119*, 4907–4922, doi:10.1002/2014JB010992.

Zhang, Q., and P. M. Shearer (2016), A new method to identify earthquake swarms applied to seismicity near the San Jacinto fault, California, *Geophys. J. Int.*, *205*(2), 995–1005.

Zhang, Y., et al. (2013), Hydrogeologic controls on induced seismicity in crystalline basement rocks due to fluid injection into basal reservoirs, *Groundwater*, *51*(4), 525–538.